MICROCOPY RESOLUTION TEST CHART
NATIONAL BUREAU OF STANDARDS-1963-A

COMPRESSIVE STRENGTH
AND DAMAGE MECHANISMS
IN PARTIALLY STABILIZED ZIRCONIA

by

James Lankford, Jr.

TECHNICAL REPORT

for

Office of Naval Research
Arlington, VA 22217

by
Southwest Research Institute
San Antonio, Texas

December 1983

DTIC
ELECTE
FEB 6 1984

A

AD A137513

DTIC FILE COPY

SOUTHWEST RESEARCH INSTITUTE
SAN ANTONIO   HOUSTON

84 01 30 024

REPORT DOCUMENTATION PAGE	READ INSTRUCTIONS BEFORE COMPLETING FORM

1. REPORT NUMBER	2. GOVT ACCESSION NO. *A137513*	3. RECIPIENT'S CATALOG NUMBER

4. TITLE (and Subtitle)	5. TYPE OF REPORT & PERIOD COVERED
Compressive Strength and Damage Mechanisms in Partially Stabilized Zirconia	Interim Technical Report 1 Aug 1982 - 31 Dec 1983
	6. PERFORMING ORG. REPORT NUMBER 06-4231

7. AUTHOR(s)	8. CONTRACT OR GRANT NUMBER(s)
James Lankford Robert Sherman	N00014-75-C-0668

9. PERFORMING ORGANIZATION NAME AND ADDRESS	10. PROGRAM ELEMENT, PROJECT, TASK AREA & WORK UNIT NUMBERS
Southwest Research Institute 6220 Culebra Road, P.O. Drawer 28510 San Antonio, TX 78284	NR 032-553/1-3-75(471)

11. CONTROLLING OFFICE NAME AND ADDRESS	12. REPORT DATE
Office of Naval Research 800 North Quincy Arlington, VA 22217	December 1983
	13. NUMBER OF PAGES

14. MONITORING AGENCY NAME & ADDRESS(If different from Controlling Office)	15. SECURITY CLASS. (of this report)
	UNCLASSIFIED
	15a. DECLASSIFICATION/DOWNGRADING SCHEDULE

16. DISTRIBUTION STATEMENT (of this Report)

This document has been approved for public release and sale; its distribution is unlimited.

17. DISTRIBUTION STATEMENT (of the abstract entered in Block 20, If different from Report)

18. SUPPLEMENTARY NOTES

19. KEY WORDS (Continue on reverse side if necessary and identify by block number)

Compressive Strength	Fracture Mechanisms	Strain-Assisted
Partially Stabilized Zirconia	Grain Boundaries	Transformation
Temperature Effects	Auger Electron Spectroscopy	Plastic Flow
Strain Rate Effects	Ceramics	

20. ABSTRACT (Continue on reverse side if necessary and identify by block number)

The flow and fracture behavior of partially (Mg) stabilized zirconia subject to compressive loading was characterized for a wide range of strain rates and temperatures. It was found that the material exhibits plastic flow from 23C to 1200C, and that the flow stress curve is serrated. Contrary to results for Al_2O_3, SiC, and Si_3N_4, the strain rate dependence of compressive strength for PSZ does not correlate with the stress intensity dependence of subcritical crack growth velocity. These results,

DD FORM 1473 JAN 73 EDITION OF 1 NOV 65 IS OBSOLETE

combined with the presence of an unusual type of deformation banding, have been interpreted in terms of plastic strain-induced, co-operative martensitic transformation of metastable precipitates.

Additional work was performed as part of an effort to establish the role of grain boundaries and grain boundary chemistry in the deformation and fracture of PSZ. Initial work has involved Auger electron spectroscopy of Ca-stabilized PSZ. It was found that intergranular regions are enriched in silica and calcium, and that grain boundary facets were apparently coated by a thin, continuous second phase film.

FOREWARD

This report describes recent work carried out under an experimental
program aimed at relating compressive damage mechanisms and compressive
failure in partially stabilized zirconia ceramics. The report consists
of three separate papers, each to be published in, or having been submitted
to, the journal noted on its title page.

TABLE OF CONTENTS

I.
PLASTIC DEFORMATION OF
PARTIALLY STABILIZED ZIRCONIA

James Lankford*
Department of Materials Sciences
Southwest Research Institute
San Antonio, Texas 78284, USA

ABSTRACT

The results of room-temperature compression experiments carried out
on polycrystalline Mg partially stabilized zirconia are described. It is
shown that in addition to prefailure axial microfracture, the material
exhibits significant plasticity. This plasticity arises from deformation
bands formed by cooperative martensitic transformation of metastable
tetragonal precipitates; the deformation bands lead to significant surface
rumpling. It is suggested that both stress- and strain-induced martensitic
transformations may be involved in the deformation process.

———

*Member, The American Ceramic Society.

INTRODUCTION

Partially stabilized zirconia (PSZ) has received considerable attention in the last few years, primarily because of its enhanced tensile strength and fracture toughness, good wear resistance, and low friction coefficient, in comparison with other technologically important ceramics such as Si_3N_4, SiC, and Al_2O_3. To date, most strength studies of PSZ have emphasized its outstanding tensile properties. However, many applications which take advantage of these properties also involve high normal (compressive) stresses; such uses include dies, wear-resistant inserts, and bearings. The purpose of this note is to present recent compression test results which have potential implications in regard to the utilization of PSZ in such situations, and which may shed some light on the martensitic transformation responsible for toughening.

EXPERIMENTAL PROCEDURES

The material chosen for study was magnesia-stabilized PSZ* with a room-temperature fracture toughness of ~8.5 MPa√m, 4-point bend strength = 600 MPa, Vickers hardness ≃ 10.2 GPa, and a grain size of ~60 μm. It is similar to an Mg-stabilized PSZ whose indentation deformation mode was reported earlier by Hannink and Swain.[1] Initial compression tests were performed at a controlled strain rate ($\dot{\epsilon}$) of ~$1 \times 10^{-4} s^{-1}$, using cylindrical

---

*Nilsen TS-Grade PSZ; Nilsen Sintered Products, Ltd, Northcote, Victoria, Australia.

specimens loaded by alumina platens.[2] Because of the non-linear behavior of the load response in these tests, duplicate experiments were carried out in load control, with crosshead displacement monitored to establish the approximate plastic strain experienced by the specimen. In addition, a few tests were carried out in displacement control at a much higher strain rate, i.e., on the order of .8s^{-1}. Acoustic emission[2] (AE) was employed as an aid in establishing the compressive damage threshold; in order to observe this damage, extremely smooth (0.05 μm diamond) flats were polished onto certain specimens prior to testing. These were loaded and unloaded below the failure level, and examined by optical microscopy.

RESULTS

Typical low strain rate results are shown in Figure 1, in which compressive stress (σ) and AE are plotted versus specimen strain ε; several points should be noted. First, the σ-ε curve exhibits a distinct plastic region, which commences at a yield strength (σ_y) of 1190 MPa. The material hardens in a more-or-less linear fashion, with failure occurring at an ultimate strength (σ_c) of 1860 MPa, and a plastic strain (ϵ_p) of 0.0124.* These yield and failure parameters are extremely repeatable, duplicate tests providing better than 1% agreement. Superimposed on the flow stress curve are local load drops which occur at irregular intervals. These

----

*This assumes that the plastic gage section is equal to the specimen length. Actually, deformation is observed to be most intense in the middle half of the speci men, so that the true plastic strain may be at least 50% higner than that indicated.
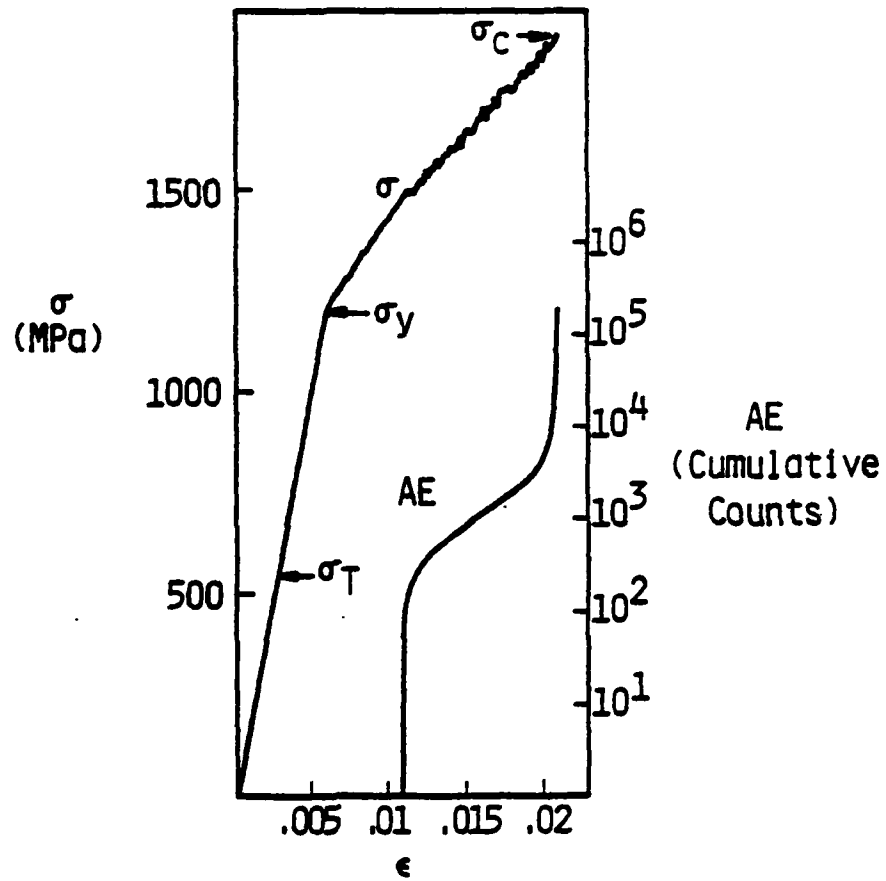
Figure 1. Compressive Stress and Acoustic Emission Versus Strain, $\dot{\epsilon} \sim 1 \times 10^{-4} s^{-1}$.

serrations are barely evident immediately upon yielding, but become steadily more pronounced as plastic deformation proceeds.

Specimens loaded to failure at the higher strain rate behaved similarly, but the strength levels increased significantly. Specifically, the yield stress in this case was approximately 1619 MPa, while the ultimate strength rose to 2073 MPa.

Evidence of deformation is readily apparent upon examining unfailed specimens loaded above the yield stress. Figure 2 shows a Nomarski contrast view of a specimen loaded to 1711 MPa (92% σ_c, $\varepsilon_p \approx 0.0085$), in which deformation bands and extensive axial microfracture are evident. Results[3] of tests at elevated temperature (~700C) indicate that AE does not occur until fracture; prior to this event (at least for $\sigma \lesssim 0.95 \sigma_c$) no micro-cracks are present, and yet the stress-strain curve is still serrated. Hence, it appears that the acoustic emission corresponds to the onset of microfracture, and is not related to the flow stress drops.

The deformation bands usually begin at grain boundaries, and frequently form as two intersecting sets within a single grain. Although the interfaces between the bands and the matrix are not perfectly straight, it appears that the bands are basically crystallographic. The bands range in size from several micrometers wide and extending across an entire grain, to short, very fine parallel laths barely discernible by optical techniques.

DISCUSSION

These features very much resemble deformation bands formed near indentations, which have recently been characterized using TEM.[1] In the latter study, Hannink and Swain observed regularly spaced bands of coarsely twinned monoclinic precipitates separated by regions of very finely
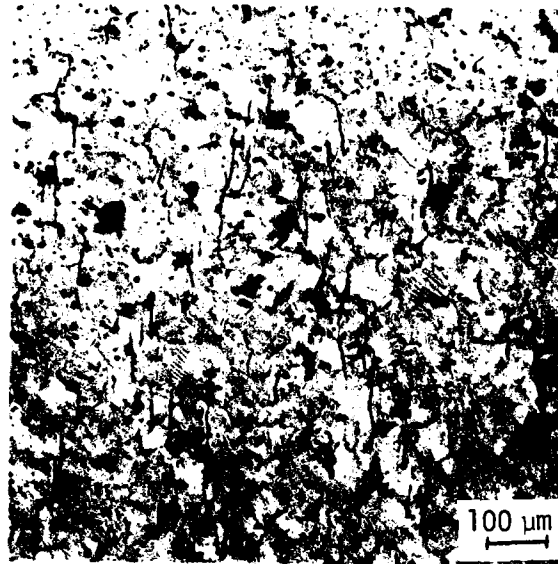
Figure 2. Axial Microfracture and Deformation Bands,
$\sigma = 1711$ MPa (92% σ_c). Nomarski contrast.

twinned monoclinic or untransformed tetragonal precipitates. It was noted that the coarsely twinned monoclinic precipitates seemed to form from favorably oriented tetragonal precipitates by a cooperative shear process; the strains associated with this shearing of many microscopic particles apparently are responsible for the macroscopic deformation bands.

The shear stresses required[1] to form the indentation slip bands are generated in predominantly compressive regions around the indent. Within such regions, shear stresses are[4] on the order of 0.1H, or 1000 MPa, which would correspond to a nominal compressive stress of ~1400 MPa. This value is reasonably close to the measured compressive yield strength of 1190 MPa, supporting the idea that the two types of deformation band are similar in nature.

It is not likely that the behavior reported for these compression experiments would be observed in bulk tensile specimens, since the tensile strength lies below the minimum stress level apparently required to generate the deformation bands (Figure 1). However, the generic martensitic reactions responsible for the deformation bands may occur within the highly-stressed vicinity of a crack tip.

Generally, the product of this type of transformation is described in the PSZ literature[5,6] as stress-induced martensite. However, certain details of the results described above suggest that this may not always be the case. In particular, studies of TRIP-steels have shown that their enhanced toughness and ductility can derive from both stress-induced and strain-induced martensitic reactions.[7,8] Stress-induced martensite forms as a direct result of elastic stresses below the actual yield strength of

the stabilized parent phase. On the other hand, martensite is strain-induced when slip in the parent precedes, and nucleates, its formation. The formation of both types of TRIP martensite is a competitive and often simultaneous process, with stress-induced transformations favored just above the "martensite-start" temperature M_s, and the strain-induced process increasingly involved as the temperature is raised.[9] Tensile and compression deformation of TRIP steels often produce serrated stress-strain curves; the serrated and smooth sections of these curves have been interpreted[8,9] in terms of competitive strain- and stress-induced martensitic transformations, respectively. Usually the internal structure of stress-induced martensite is identical to that in martensite which occurs spontaneously below M_s, but different from that observed in strain-induced martensite.[9]

In the present case, serrations are superimposed upon an initially smooth flow stress curve, suggesting that two types of plasticity may be occurring simultaneously. Assuming that the stable cubic matrix itself is not flowing, then the plasticity must be associated with transformation of the metastable tetragonal precipitates to the monoclinic structure. It would thus appear that competing stress- and strain-induced martensitic transformations may be responsible for the observed stress-strain behavior. Recalling the TEM observations of Hannink and Swain,[1] this seems plausible, since they report two monoclinic variants, i.e., "coarsely" twinned, and "very finely" twinned. One of these would correspond to strain-induced martensite, and the other to stress-induced and/or spontaneously transformed (on cooling) martensite; based on TRIP steel research,[7] the latter would be identical.

The idea that strain-induced martensite may be involved in the compressive damage of PSZ is further supported by the fact that the yield strength increases with strain rate. Yielding due to a stress-induced transformation should be rate independent, while strain-induced transformations are dependent upon strain rate through the requirement that thermally-activated slip in the parent tetragonal phase precede its subsequent rate independent martensitic transformation.

Evaluation of the validity of these inferences regarding the nature of the TRIP processes in PSZ during compressive loading requires further experimentation. Critical tests involve varying compressive strain rate and temperature over wide ranges, and characterizing resultant damage processes at higher resolution, using transmission electron thin foil and replica microscopy. Such experiments are in progress.

Regardless of the details of the compressive deformation process, its effect upon certain applications of PSZ may be important. Figure 3 is an oblique light view of the same area shown in Figure 2; it is evident that the surface is extremely rumpled, corresponding to a significant increase in the effective surface roughness. It should be appreciated that this surface was initially extremely smooth and flat. Such roughness, induced during the type of compressive service loading involved, for example, in bearings, could have a decidedly detrimental effect upon service life. If the principal process involved in the generation of the deformation bands is indeed a strain-induced martensitic transformation, then the corresponding surface roughness would tend to increase as the operating temperature rises relative to M_s.
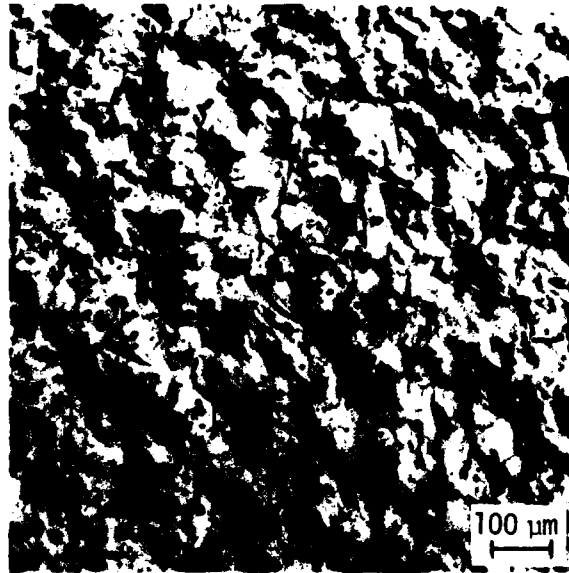
Figure 3. Surface Rumpling Due to Deformation Bands. Oblique light view of same region shown in Figure 2.

CONCLUSIONS

1. Mg-stabilized PSZ exhibits serrated plastic flow during compression at room temperature.

2. The flow stress is strain rate sensitive.

3. The TRIP processes responsible for plastic deformation bands may involve both stress-induced and strain-induced martensitic reactions.

4. The deformation bands produce significant surface rumpling.

ACKNOWLEDGEMENTS

REFERENCES

1. R. H. J. Hannink and M. V. Swain, "A Mode of Deformation in Partially Stabilized Zirconia," J. Mat. Sci., 16 [5] 1428-1431 (1981).

2. J. Lankford, "Uniaxial Compressive Damage in α-SiC at Low Homologous Temperatures," J. Am. Cer. Soc., 62 [5-6] 310-312 (1979).

3. J. Lankford, "The Effect of Temperature and Loading Rate on Compressive Damage and Failure in Partially Stabilized Zirconia," J. Mat. Sci. (submitted).

4. J. T. Hagan, "Micromechanics of Crack Nucleation During Indentation," J. Mat. Sci., 14 [12] 2975-2980 (1979).

5.   A. G. Evans and A. H. Heuer, "Transformation Toughening in Ceramics: Martensitic Transformations in Crack-Tip Stress Fields," J. Am. Cer. Soc., 63 [5-6] 241-248 (1980).

6.   D. L. Porter, A. G. Evans, and A. H. Heuer, "Transformation-Toughening in Partially-Stabilized Zirconia," Acta Met., 27 [10] 1649-1654 (1979).

7.   P. C. Maxwell, A. Goldberg, and J. C. Shyne, "Stress-Assisted and Strain-Induced Martensites in Fe-Ni-C Alloys," Met. Trans., 5 [6] 1305-1318 (1974).

8.   D. Fahr, "Stress- and Strain-Induced Formation of Martensite and Its Effect on Strength and Ductility of Metastable Austenitic Stainless Steels," Met. Trans., 2 [7] 1883-1892 (1971).

9.   P. C. Maxwell, A. Goldberg, and J. C. Shyne, "Influence of Martensite Formed During Deformation on the Mechanical Behavior of Fe-Ni-C Alloys," Met. Trans., 5 [6] 1319-1324 (1974).

II.
THE INFLUENCE OF TEMPERATURE AND LOADING RATE ON
FLOW AND FRACTURE OF PARTIALLY STABILIZED ZIRCONIA

James Lankford

Department of Materials Sciences
Southwest Research Institute
San Antonio, Texas 78284, USA

The flow and fracture behavior of Mg stabilized partially stabilized zirconia subject to compressive loading is characterized for a wide range of strain rates and temperatures. It is found that the material exhibits plastic flow from 23C to 1200C, and that the flow stress curve is serrated. Contrary to results for Al_2O_3, SiC, and Si_3N_4, the strain rate dependence of compressive strength for PSZ does not correlate with the stress intensity dependence of subcritical crack growth velocity. These results, combined with the presence of an unusual type of deformation banding, are interpreted in terms of plastic strain-induced, cooperative martensitic transformation of metastable precipitates.

Introduction

Recently, the author reported[1] the results of a study of the compressive behavior of partially stabilized zirconia (PSZ). The experiments, performed at room temperature and moderate loading rates, demonstrated that failure was preceded by significant plastic flow, behavior which is uncharacteristic of tensile fracture. It was found that this plasticity resulted from unusual deformation bands, and suggested that the latter form by the cooperative, strain-induced martensitic transformation of metastable tetragonal precipitates.

However, many potential applications (bearings, engine components) of partially stabilized zirconia involve a compressive state of stress, rapid loading, and temperatures between 23C and ~1000C. Furthermore, it already is known that elevated temperatures tend to degrade the outstanding te. 'le strength and fracture toughness which PSZ exhibits under ambient conditions. This paper therefore describes the results of an investigation which extends the previous compressive work into the projected operational regime.

Experimental Procedures

The same Mg stabilized ceramic* studied earlier[1] was used in the present experiments; material and mechanical properties are characterized in Table I. Specimens were provided in the form of as-sintered right circular cylinders, with a length of .625 cm, and a diameter of .3125 cm. Special care was taken to precision grind and lap parallel to within 2 µm the ends of both the specimens and their alumina loading platens.

Compression tests were performed at strain rates ranging from $7 \times 10^{-5} s^{-1}$ to $1 \times 10^3 s^{-1}$; low and intermediate rates were achieved using a standard servo-controlled test machine, while the fastest tests were accomplished by means of a Hopkinson pressure bar system. Since the load response of the material was found to be nonlinear, duplicate experiments were performed in load control, for low loading rates, with crosshead displacement monitored in order to characterize the approximate plastic strain prior to failure. Elevated temperature tests (to ~1200C) were run in a resistance-heated furnace within a dry argon environment.

---

*Nilsen TS-Grade PSZ; Nilsen Sintered Products, Ltd, Northcote, Victoria, Australia.

TABLE I

AMBIENT MATERIAL AND MECHANICAL PROPERTIES*

Tensile Strength (4 bend) (MPa)	Vickers Hardness (GPa)	Fracture Toughness (MPa$\sqrt{m}$)	Grain Size (μm)
600	10.2	8-15**	~60

*Data from Nilsen Sintered Products, Ltd.

**Toughness variable due to R-curve behavior.

In order to establish the threshold stress level for microfracture, acoustic emission (AE) was employed. The PZT transducer, resonant at 160 kHz, operated within the frequency range 100 kHz to 1 MHz. Since high temperatures were involved, the transducer was affixed to the loading ram; ambient environment experiments indicated that the signal amplitude due to microfracture events was not significantly reduced by positioning the trans-ducer away from the specimen itself.

Optical and scanning electron microscopy were used to characterize damage mechanisms and post-failure fractography. In order to accomplish the former, extremely smooth (0.05 µm diamond finish) flats were polished onto certain specimens prior to testing. These were loaded to stress levels above yield, but below the ultimate strength, unloaded, and in-spected microscopically. Specimens were coated with palladium in order to enhance optical contrast, and to permit SEM study.

Finally, the hardness of the PSZ was determined as a function of temperature to 800C. Hardness tests were performed using a modified Tukon microhardness tester; the specimen and Vickers diamond pyramid indenter were immersed in argon and heated by a small resistance furnace. Indenter loads ranged from 200-800 gms, over which range hardness was approximately independent of load.

Results

The effect of temperature (T) on compressive strength (σ_c) for strain rates ($\dot{\epsilon}$) of $7 \times 10^{-5} s^{-1}$, $.2 s^{-1}$, and $10^3 s^{-1}$, are shown in Figure 1; also shown is the temperature dependence of the acoustic emission damage thresh-old (σ_{AE}) for $\dot{\epsilon} = 7 \times 10^{-5} s^{-1}$. At low and intermediate loading rates,
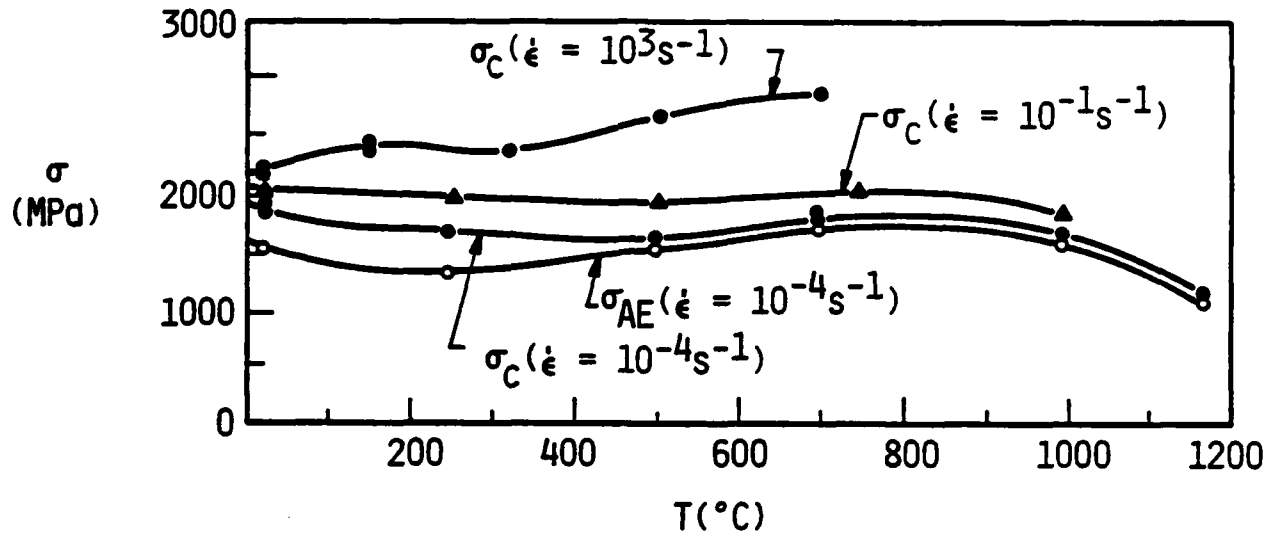
Figure 1. Compressive strength (σ_C) and damage threshold stress level (σ_{AE}) versus temperature.

strength is essentially independent of temperature for T≲1000C, above which the strength at $\dot{\varepsilon} = 7\times10^{-5}s^{-1}$ begins to drop. Conversely, σ_c increases monotonically with T at $\dot{\varepsilon} = 10^3s^{-1}$ over the temperature range studied, i.e., to 700C. It is interesting to notice the extremely good repeatability of the strength measurements; duplicate tests yield σ_c values which agree within ~1%. This probably is a consequence of the fact that the specimens yield prior to failure, behaving more like metals rather than classical brittle ceramics.

The acoustic emission results for the lowest strain rate roughly parallel the corresponding compressive strength. However, σ_c and σ_{AE} diverge for T≲500C, indicating that microfracture events precede gross failure. Convergence of σ_c and σ_{AE} above 500C suggests either that pre-failure microfracture does not occur, or that such events are different in nature from those which take place at lower temperatures, and do not provide significant AE. As will be seen, microscopy indicates that the latter is in fact the case.

It is helpful also to plot the strength data in terms of $\dot{\varepsilon}$, as shown in Figure 2 for T = 23C; also shown are equivalent results* for other ceramics tested previously[2] by the author. Like these other materials, PSZ exhibits a linear log σ_c-log $\dot{\varepsilon}$ dependence,** and as for Al_2O_3 and NC 350 ($\dot{\varepsilon} \lesssim 10^1s^{-1}$), the slope of the PSZ relationship is low, but measurable. The significance of this parameter will be considered in the next section.

As mentioned earlier, PSZ tends to flow under the high stresses tolerated by compressive loading. Shown in Figure 3 are the compressive

---

*The behavior for $\dot{\varepsilon} \gtrsim 10^3s^{-1}$ is discussed elsewhere.[2]

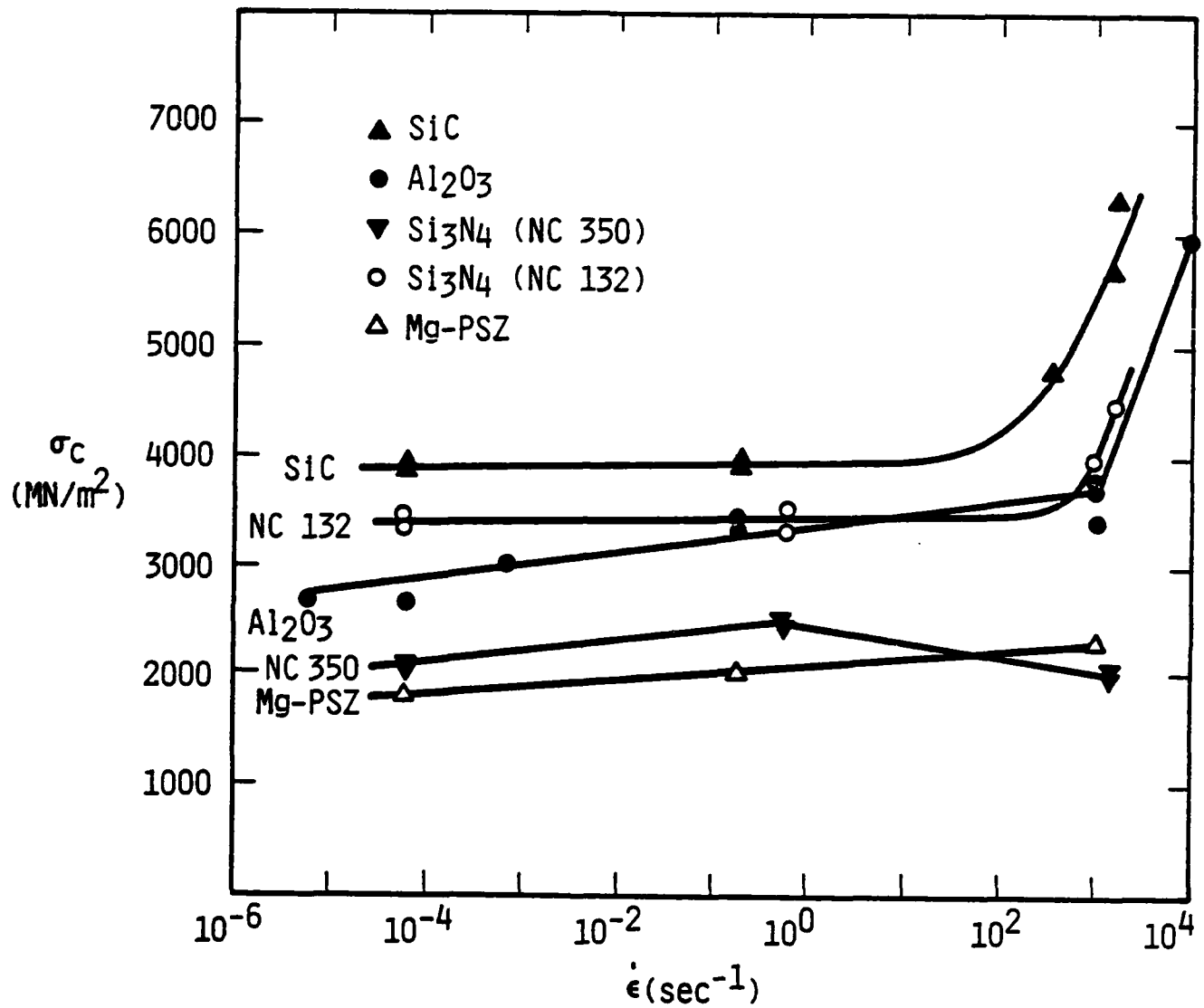**Figure 2 is plotted as σ-log $\dot{\varepsilon}$ in order to emphasize the slope.

Figure 2.   Compressive strength versus strain
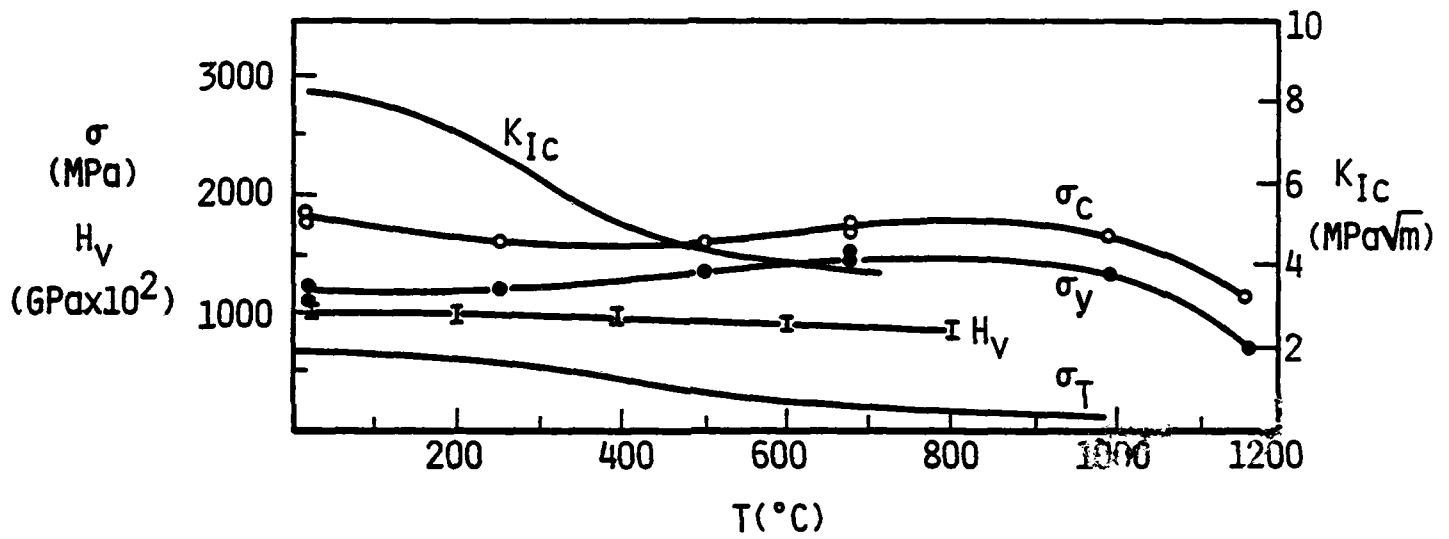rate for various ceramics, T = 23C.

Figure 3. Fracture toughness, compressive strength, yield strength, tensile strength, and hardness versus temperature.

strength and the yield strength (σ_y; defined as the apparent proportional limit) versus temperature for $\dot{\varepsilon} = 7 \times 10^{-5} s^{-1}$. Also plotted are the fracture toughness[3] (K_{IC}), the hardness (H_v), and the 3-point bend strength[4] (σ_T).

Although fracture toughness decreases quickly over the range 23C < T < 500C, the other properties are much less sensitive to temperature until T≳1000C. Below 1000C, the plastic strain prior to failure averages 1.5%, over which range considerable strain hardening occurs, i.e., σ_c/σ_y ranges from 1.27 to 1.5. As for σ_c, the tensile strength experiences a significant decrease once T exceeds 1000C.

The plastic flow behavior is complicated by transient load drops superimposed upon the strain hardening curve. This behavior was demonstrated elsewhere[1] for ambient conditions; as shown in Figure 4, it persists at elevated temperatures as well. The figure represents an actual experimental load-time trace for T = 1000C, which shows that the serrations do not occur instantly after yielding, and that the failure strength is lower than the ultimate stress (σ_{ULT}) achieved in the test. At higher temperatures, the latter effect increases, until at 1168C, for example, $\sigma_{ULT}/\sigma_c \cong 1.2$. In addition, the serrations occur more frequently, and involve larger load drops, at higher temperatures.

Considerable insight regarding the basis of this behavior can be derived from microscopy. As shown for T = 23C in Figure 5, the strain-hardening, serrated flow stress region corresponds to the formation of axially-oriented transgranular microcracks, and what appear to be some sort of deformation bands. At higher temperatures, i.e., T≳600C, the same situation prevails, with the exception that most of the axial microcracks now tend to lie along grain boundaries; the transition to intergranular microfracture is complete above ~1000C.

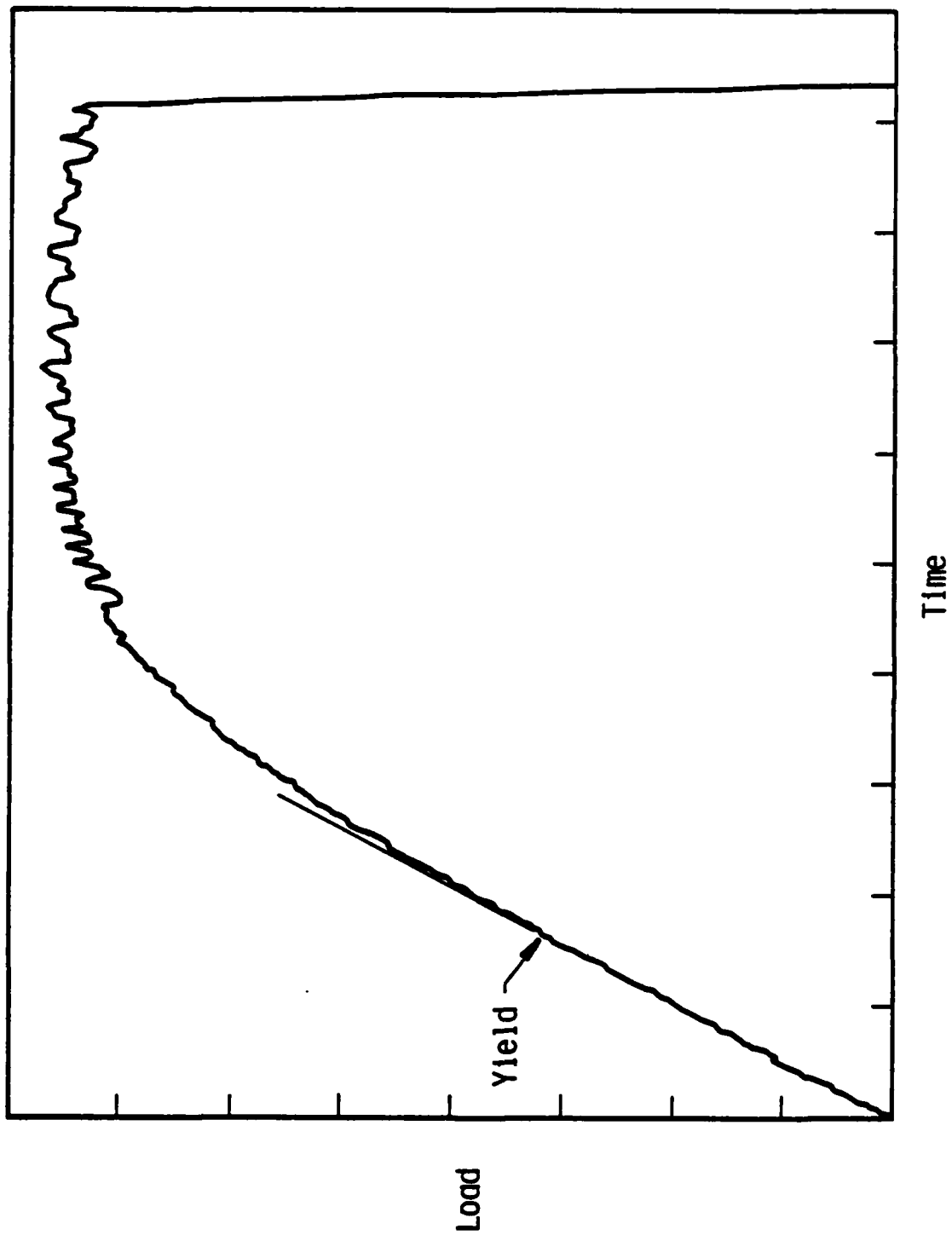Figure 4. Serrated load versus time curve for $\dot{\varepsilon} = 7 \times 10^{-5} s^{-1}$ and T = 1000C.

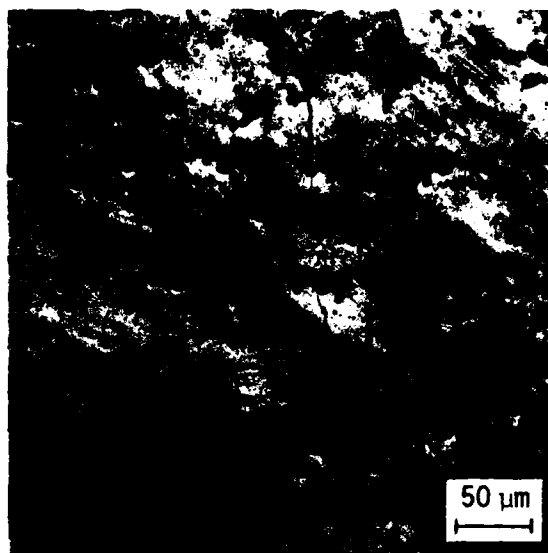Figure 5. Transformation bands and axial microfracture; $T = 23C$, $\sigma \simeq 90\%$ σ_c, $\varepsilon \simeq 0.012$.

It is interesting to observe that the deformation bands, which are so strikingly visible in Nomarski optical illumination, are almost invisible in the SEM. The edges of the bands, in particular, are nearly indiscernible, suggesting that they do not consist of discrete ledges, and so differ from classical slip bands. The edges of the latter enhance secondary electron emission, and generally show up quite well in the SEM.

Optical examination and monitoring of acoustic emission indicates that the onset of axial microfracture correlates with the threshold stress for acoustic emission. Deformation bands begin to form in favorably oriented grains below this stress level, while the load drops in the stress-strain curve seem to correspond to prolific banding and associated surface rumpling[1] within the bulk of the specimen. In this regime, inserting bands are formed due to the activity of multiple "flow" systems within individual grains.

Discussion

Transgranular microfracture apparently is responsible for pre-failure acoustic emission at T≲500C. Although intergranular microfracture likewise precedes failure at higher temperatures, this is a "quiet" process, which probably means that it takes place via grain boundary sliding, rather than rapid tensile rupture. This is borne out by the fact that SEM analysis of specimens unloaded just prior to failure at 1000C showed that many surface grains already had extruded several μm out of originally smooth surfaces.

The author has shown elsewhere[2] that for $\dot{\varepsilon} \gtrsim 10^2 s^{-1}$, $\sigma_c(\dot{\varepsilon})$ tends to follow a relationship of the form

$$\sigma_c \propto \dot{\epsilon}^{1/1+n_c} \tag{1}$$

where $n_c \approx n$ (Table II), the exponent in the crack growth relationship

$$V = AK^n \tag{2}$$

Here V is the growth velocity of a Mode I tensile crack in a fracture mechanics-type specimen, K is the stress intensity, and A is a material and environment-dependent constant. It already is well known that the failure of an unflawed brittle ceramic specimen tested in bending obeys a $\sigma_T(\dot{\epsilon})$ relationship of the form

$$\sigma_T \propto \dot{\epsilon}^{1/1+n_T} \tag{3}$$

in which the measured equivalence between n_T and n is accepted as proof that the strength-strain rate dependence is based upon thermally activated, tensile microcrack growth.

As shown in Table II, the behavior of Mg-PSZ clearly violates the trend shown by the other materials listed. Although $n \approx n_T$, as expected, n_c is nearly twice n, suggesting that something other than, or in addition to, subcritical crack growth, is responsible for the temperature dependence of n. Based on the observation of "deformation bands," and the serrated nature of the stress-strain curve, it seems likely that this other thermally activated mechanism is related to dislocations. Although this conclusion might seem rather inevitable, close consideration shows that the situation is rather more complex than it appears.

TABLE II

COMPARISON OF STRENGTH-STRAIN RATE AND CRACK
VELOCITY-STRESS INTENSITY EXPONENTS

Material	$n(K-V)$	n_T (Dynamic Bending Fatigue Test)	n_C (Compression)
Al_2O_3	52^5	--	51
NC 350	57^6	--	52
NC 132	very large[6]	--	very large
SiC	very large[7]	--	very large
Limestone	130^8	--	143^{11}
Mg-PSZ	50-55[9]*	46-68[10]	95

---

*Li and Pabst[9] report an n value of 80 for K-V specimens with as-machined, residual-stressed surfaces; elimination of this machining damage by annealing yielded "true" n values of 50-55.

For example, it is thought that the enhanced fracture toughness of PSZ at ambient temperatures is caused by the free energy[12] of, or residual stress fields[13] associated with, the crack tip stress-assisted[14,15] phase transformation of metastable precipitates from the tetragonal to the monoclinic structure. As the temperature rises, both the free energy associated with this martensitic transformation, and K_c, decrease, until at approximately 600C, the net energy of transformation is negligible, and K_c no longer decreases (Figure 3). However, the transformation itself nevertheless persists to higher temperatures, and since there is always a shape change associated with the transformation, this might arguably account for the plasticity observed in the present experiments.

However, stress-induced martensitic transformations are strain rate independent. This suggests, as proposed earlier by the author[1] and, independently, Hannink and Swain,[16] that the deformation bands produced under compressive loading are caused by a strain-induced[17,18] martensitic reaction. In this case, the transformation is initiated by the microstress fields of dislocations nucleated within the cubic matrix and/or the tetragonal parent phase. The dislocations are envisaged to progress avalanche-fashion along zones of high shear stress, producing "deformation bands" of transformed material. Production of each band, or set of bands, would correspond to a load drop, and produce an increment of plastic strain.

The apparent structure of the transformation bands is sketched in Figure 6. Hannink and Swain[19] have performed transmission electron microscopy on Mg-PSZ deformation bands identical in appearance to those reported, but produced in the compressive zones adjacent to indentations. Although the bands are composed of transformed monoclinic particles within
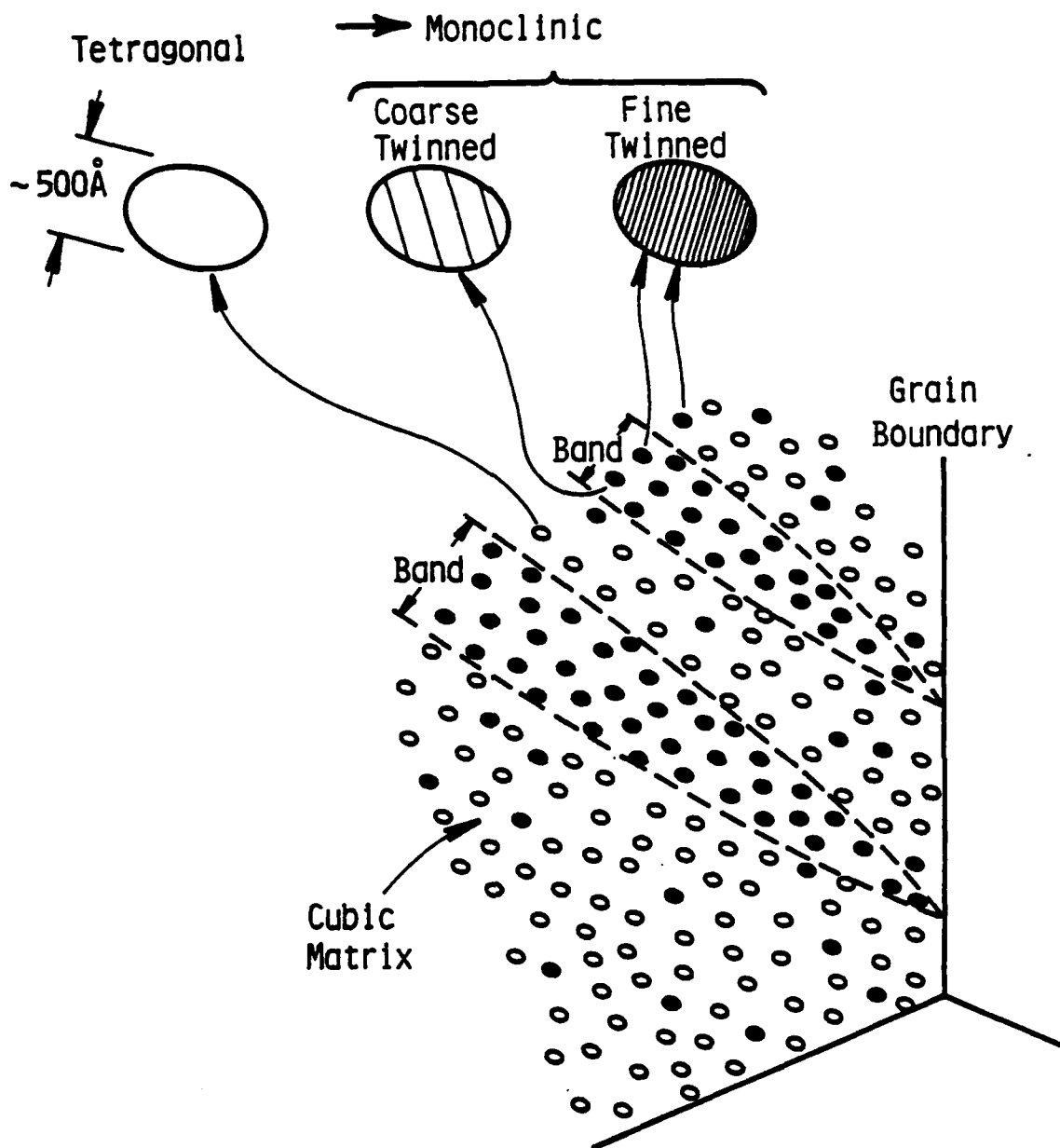
Figure 6. Conceptual sketch of strain-induced cooperative transformation
bands. Coarse-twinned monoclinic precipitates are strain-
induced, and lie only within deformation bands. Fine-twinned
particles formed during cooling below M_S, and possibly as a
result of compressive stress-assisted transformation, and are
therefore found throughout the microstructure.

a cubic matrix, the particles are characterized by two distinct internal microstructures. The first variant is coarse twinned, and found only inside the deformation bands; the second, fine-twinned type of monoclinic precipitate is located both within and without the bands.

An analogous situation is found in steels toughened by means of transformation-induced plasticity (TRIP). Deformation of these steels produces serrated stress-strain curves, the smooth sections of which are interpreted[18,20] in terms of (elastic) stress-assisted martensitic transformations, and the serrations in terms of (plastic) strain-induced transformations. It is generally found that the internal microstructure of stress-assisted martensite is identical to that which occurs spontaneously on cooling below M_s, but differs markedly from that characteristic of strain-induced martensite. Also, the strain-induced process becomes increasingly prevalent as the temperature of the deformation process rises.[20]

In the case of Mg-PSZ, the presence of two transformation variants within the deformation bands clearly suggests that a strain-induced martensitic process is responsible for the bands. This is supported by the fact that the serrations become larger and more frequent with increasing temperatures, corresponding to increasingly easier dislocation activation. The fact that the band edges are so indistinct when viewed in the SEM can be understood in terms of their structure. As shown in Figure 6, the bands are composed of an ensemble of transformed regions within an untransformed matrix; hence, their is no continuous boundary line analogous to a slip line.

To date, no TEM evidence for dislocation flow in PSZ has been observed.[19,21] However, the search for dislocations in the complex and highly strained microstructure is very difficult,[19] and the defects may be annihilated during the transformation process itself. Further research in this area is required.

Conclusions

It was found that the compressive behavior of Mg-PSZ is unique relative to other strong ceramics. In particular, the material exhibits a serrated stress-plastic strain curve at all temperatures studied, and a strength-strain rate dependence which does not correlate with K-V experiments. Cooperative transformation deformation bands form at all test temperatures. These results suggest that strain-induced martensitic transformations are important in high stress situations such as compression and indentation, while stress-assisted transformations probably are more relevant to crack tip (toughening) processes.

Acknowledgements

References

1. J. Lankford, J. Amer. Ceram. Soc. 66 (1983) C-212.

2. J. Lankford, Frac. Mech. Ceram., Vol. 5, Ed. R. C. Bradt, A. G.
    Evans, D. P. H. Hasselman, and F. F. Lange, Plenum Press, N.Y.
    (1983) 625.

3. M. V. Swain (private communication).

4. M. Marmach, D. Servent, R. H. J. Hannink, M. J. Murray, and M. V.
    Swain, "Toughened PSZ Ceramics - Their Role as Advanced Engine
    Components," SAE Technical Paper 830318 (1983).

5. A. G. Evans, M. Linzer, and L. R. Russell, Mat. Sci. Eng. 15 (1974)
    253.

6. K. D. McHenry, T. Yonushonis, and R. E. Tressler, J. Am. Cer. Soc.
    59 (1976) 262.

7. K. D. McHenry and R. E. Tressler, J. Am. Cer. Soc. 63 (1980) 152.

8. J. P. Henry, J. Paquet, and J. P. Tancrez, Int. J. Rock Mech. Min.
    Sci. & Geomech. Abstr. 14 (1977) 85.

9. L. S. Li and R. F. Pabst, J. Mater. Sci. 15 (1980) 2861.

10. J. D. Helfinstine and S. T. Gulati, Ceram. Bull. 59 (1980) 646.

11. S. J. Green and R. D. Perkins, Proc. 10th Sym. Rock Mech., Ed.
    K. E. Gray (1968) 35.

12. F. F. Lange, "Research of Microstructurally Developed Toughening
    Mechanisms in Ceramics," ONR Technical Report, Contract No.
    N00014-77-C-0441, June 1982.

13. R. M. McMeeking and A. G. Evans, J. Amer. Ceram. Soc. 65 (1982) 242.

14. A. G. Evans and A. H. Heuer, "Transformation Toughening in Ceramics:
    Martensitic Transformations in Crack-Tip Stress Fields," J. Am. Cer.
    Soc. 63 [5-6] (1980) 241-248.

15.   D. L. Porter, A. G. Evans, and A. H. Heuer, "Transformation-
Toughening in Partially-Stabilized Zirconia," Acta Met. 27 [10]
(1979) 1649-1654.

16.   R. H. J. Hannink and M. V. Swain, Proc. Int. Sym. Plas. Def. Ceram.,
July 1983, Penn. St. Univ. (in press).

17.   P. C. Maxwell, A. Goldberg, and J. C. Shyne, "Stress-Assisted and
Strain-Induced Martensites in Fe-Ni-C Alloys," Met. Trans. 5 [6]
(1974) 1305-1318.

18.   D. Fahr, "Stress- and Strain-Induced Formation of Martensite and
Its Effect on Strength and Ductility of Metastable Austenitic
Stainless Steels," Met. Trans. 2 [7] (1971) 1883-1892.

19.   R. H. J. Hannink and M. V. Swain, J. Mat. Sci. Letters 16 (1981)
1428.

20.   P. C. Maxwell, A. Goldberg, and J. C. Shyne, "Influence of
Martensite Formed During Deformation on the Mechanical Behavior of
Fe-Ni-C Alloys," Met. Trans. 5 [6] (1974) 1319-1324.

21.   A. H. Heuer (private communication).

III.
AUGER ANALYSIS OF A CALCIUM PARTIALLY STABILIZED ZIRCONIA

by Robert Sherman

Partially stabilized zirconia (PSZ) offers unique properties compared to other strong ceramics, especially in terms of fracture toughness. This increased toughness is due to the crack tip stress-assisted martensitic transformation of tetragonal phase precipitates to the monoclinic phase.[1] The large volume expansion and resulting compressive stresses are believed to retard growing cracks in PSZ.

A limitation in applying ceramics is the inherent weakness of grain boundaries due to solute segregation, porosity, and discrete or continuous second phases. For an yttria PSZ, Rice, et al.[2] have shown that grain boundaries are often sites of fracture initiation. The PSZ in their study contained extensive grain boundary porosity, but it was argued that pores were not solely responsible for fracture initiation. Instead, Rice suggested that a combination of porosity and grain boundary chemistry may be responsible for the inherent weakness of polycrystalline samples when compared to single crystals. Lenz and Heuer[3] examined magnesium and calcium PSZs that underwent subcritical crack growth in water and observed intergranular crack growth at low stress intensities and transgranular crack growth at high stress intensities. The possible effects of grain boundary chemistry were suggested as being at least partially responsible for the differences in crack path.

This study was carried out to investigate the grain boundary chemistry of a calcium PSZ. Auger Electron Spectroscopy (AES) was used to determine the differences and similarities between intergranular and transgranular compositions.

The material investigated was a 3.7 wt.% calcium PSZ prepared by Dr. M. V. Swain (CSIRO, Australia). The specimen was cooled from the solid solution region in a controlled fashion, such that metastable precipitates developed in a cubic matrix. The sample was heated at 1300°C for about 40 hours so that the resulting structure was partially stabilized (metastable tetragonal and transformed monoclinic particles within a cubic matrix).

Auger analysis was performed with a Physical Electronics 595 scanning Auger microprobe at a background pressure of about 2.6×10^{-8} Pa (2×10^{-10} torr). The sample was fractured at a high strain rate in vacuum immediately preceeding analysis. Typical spectra, elemental maps, and depth profiles were obtained with an incident electron beam voltage of 3 keV and electron beam current of 10nA (1×10^{-8}A). Low accelerating voltage and beam currents were used to prevent the sample from developing a charge during analysis. All displayed Auger spectra were acquired in the multiplex mode to increase the signal-to-noise ratio. General surveys over the entire applicable energy range were acquired initially and were used as guides to set up the higher resolution multiplex mode. Auger depth profiling was performed using 4 keV argon ions rastered over an area of about 1mm^2. The sputter rate was estimated to be .025 nm/sec and was based upon the time required to sputter through a 100 nm SiO_2 thin film.

A typical example of the microstructure is shown in Figure 1. The fracture surface was mostly transgranular, but several intergranular facets were observed and both regions exhibited extensive porosity. Intergranular porosity was located on grain surfaces, triple lines, and grain boundary vertices (triple points). Transgranular pores appeared smaller for the most part

Figure 1. Micrograph of the fracture surface of Ca-PSZ.

(though examples of larger transgranular pores were seen and are discussed later).

Auger spectra from both transgranular and intergranular regions are shown in Figure 2. Inspection of Figure 2 indicated the presence of oxygen, calcium, zirconium and silicon on the intergranular fracture surface while the transgranular fracture surface exhibited evidence of only oxygen, calcium, and zirconium. An enhancement of the calcium concentration by about a factor of four was observed on all intergranular facets, independent of the amount of porosity.

The spectra for both silicon and zirconium indicated that they were in an oxide chemical state, not an elemental state (no chemical state information can be deduced from the calcium peak shape). This conclusion was based upon comparison of our spectra with other published spectra. The identification of silicon as an oxide[4] was based upon the peaks at 79 eV, 65 eV, and a weak peak at 1612 eV (not shown).

The identification of the zirconium peaks as zirconium oxide was based upon comparison of the spectra in Figure 2 with published spectra of elemental and oxidized zirconium.[4,5,6] A peak at 147 eV dominates the Auger spectrum of elemental zirconium, and side peaks occur at 174, 128, 120, and 92 eV. Upon oxidation, Auger peaks involving valence electrons (127, 147, and 174 eV) of elemental zirconium were strongly attenuated, while Auger peaks involving core electrons (92 and 120 eV) were not attenuated. Also, peak shifts of several electron volts to lower energies were observed.[6]

The transgranular spectrum in Figure 2b indicated peaks at 90, 114, 127, and 142 eV, and the peak locations and shapes agreed well with the data from Krishan et al.[6] The peak at 149.5 eV was believed to be due to electron
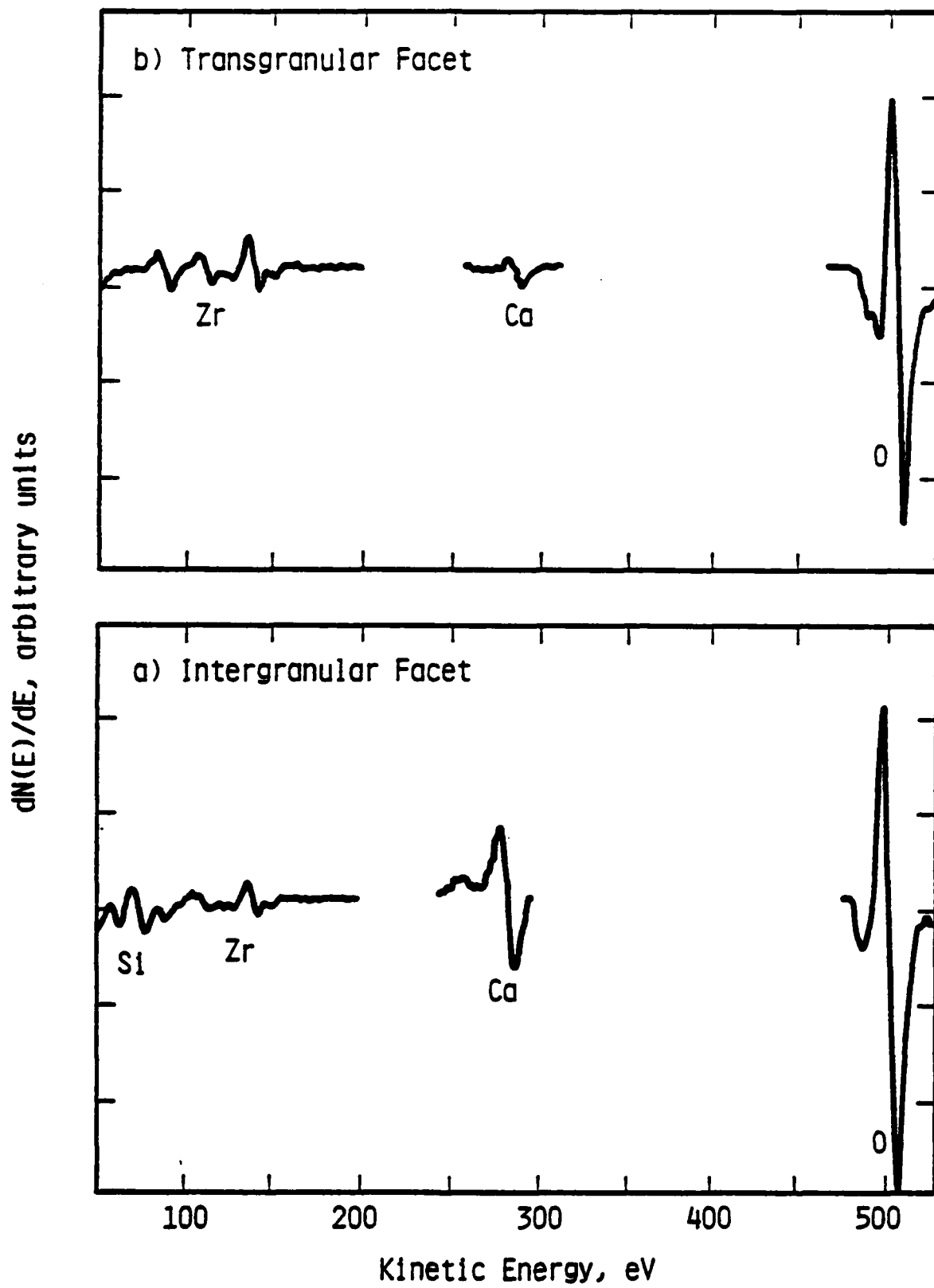
Figure 2. Auger spectra from a) intergranular and b) transgranular regions.

beam decomposition of the zirconia. By observing the secondary electron counts in real time, it was possible to monitor growth in the 149.5 eV peak at the expense of the 142 eV peak. With this small change in the 149.5 eV peak, changes due to excessive electron beam currents in the other zirconium peaks were not expected.

A high energy peak for zirconium is known to exist at 1845 eV.[4] Spectra from transgranular regions of the sample indicated that a peak shift to lower energies occurred to approximately 1835 eV. The shift in energy of the high energy zirconium peak is similar to what has been observed for other metal oxides.[4] Peak shape changes are not discussed due to the weakness of this high energy peak and the resulting low signal-to-noise characteristics of the spectra at high energies.

Depth profiles were obtained from both transgranular and intergranular facets. As discussed below, major changes in surface chemistry occurred during depth profiling of an intergranular facet, while no major changes occurred during depth profiling of a transgranular region.

The depth profile for calcium from an intergranular facet is shown in Figure 3. A decrease in the calcium peak-to-peak height by about a factor of four was observed as the sputter time increased. With a sputter rate of .025 nm/sec, a thickness of 1.0 nm was calculated for the calcium layer on the grain facet. If one assumed that fracture occurred down the center of the this layer, then a 2.0 nm layer exists on the grain facets. The silicon peak at 76 eV displayed similar behavior during the depth profile.

As mentioned earlier, porosity was observed on both intergranular and transgranular regions of the fracture surface. Auger spectra acquired from
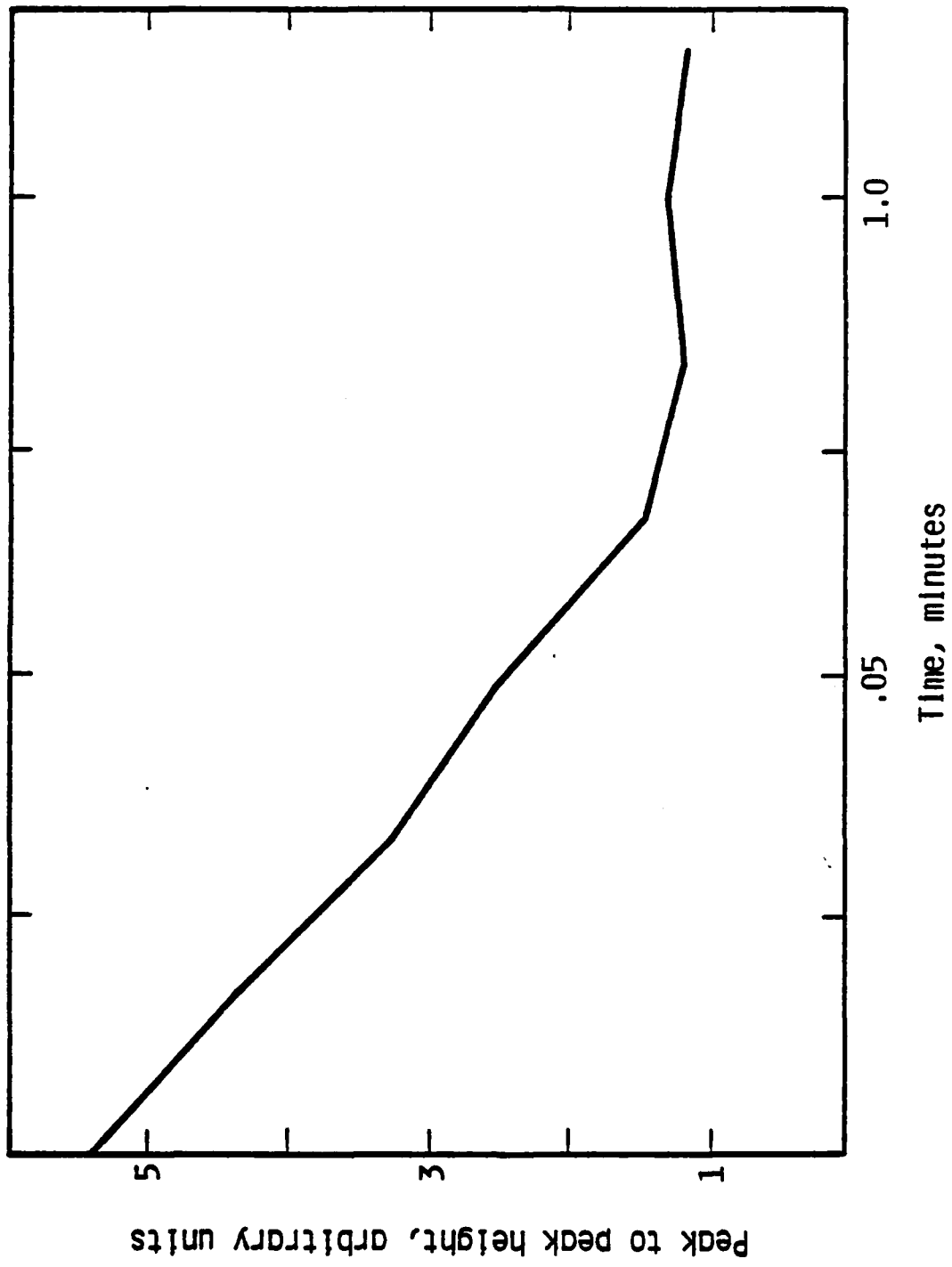
Figure 3. Depth profile for calcium from an intergranular facet.

pores on both intergranular and transgranular facets displayed similar chemistries to those of smooth regions on an intergranular facet. In Figure 4a, a micrograph of about twelve pores is shown. These pores are predominantly transgranular, with some possibly related to a grain boundary trace. In Figure 4b, an Auger elemental map for calcium is shown. Excellent agreement between the pores in the micrograph and the location of strong intensity in the elemental map (indicating a high calcium concentration) was observed.

The above results indicate there is a difference between transgranular and intergranular chemistry. Additional silicon and calcium on the grain facets may be due to a segregated layer or to a continuous second phase. The mechanism responsible for enhancements of calcium and silicon is not known, but the ceramic literature does indicate that processing methods may be responsible.

Calcium segregation to grain boundary facets has been observed in many other ceramic systems,[7,8] but for this PSZ, solute segregation may not be responsible for the calcium enhancement. Drennan[9] states that for calcium and magnesium PSZs, silica leaches the stabilizer from the zirconia even at low impurity levels. The increased calcium signal on the grain facets may be due to a chemically driven dissolution phenomenon rather than solute segregation.

Silica is a common impurity in zirconia ceramics, especially since zirconia forms a stable silicate, zircon, with silica. Silica, in additions up to several wt. percent, has been added as a sintering aid to PSZ's, and can react with the bulk calcia to form a glassy grain boundary phase.[10] The
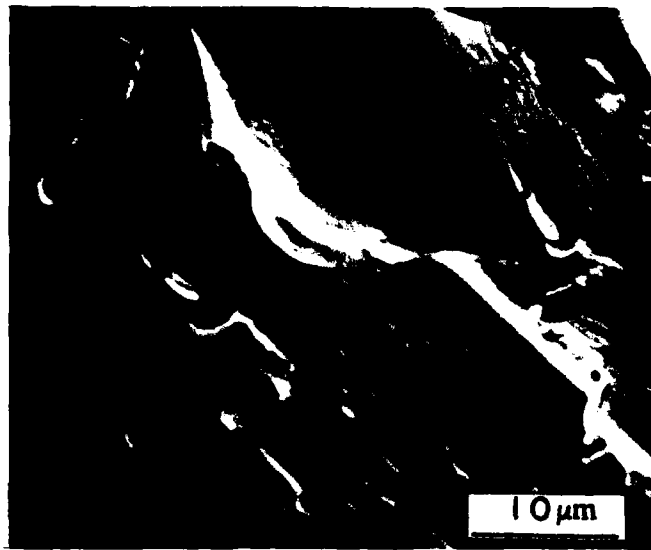
(a)
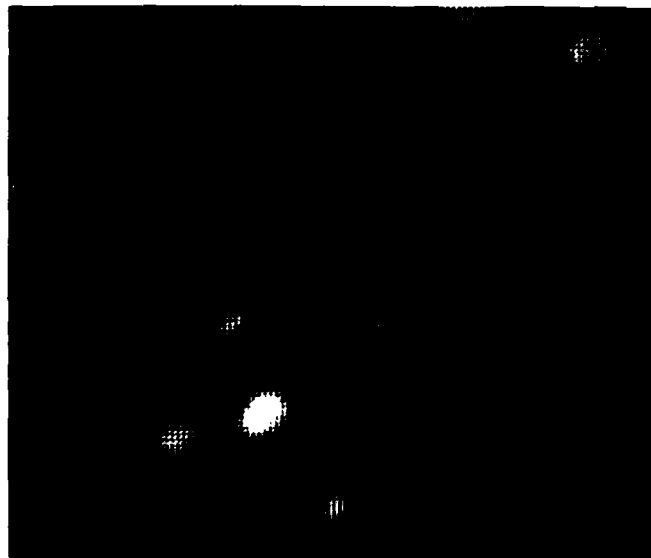
(b)

Figure 4. a) Auger micrograph showing extensive transgranular
porosity and b) corresponding calcium elemental map.

Auger results can be understood if silica can act as a sintering aid when present as a residual impurity. The silica, present on grain facets during various stages of sintering, will react with bulk calcium, especially during grain growth, to yield a thin continuous grain boundary phase.[11]

Transmission electron microscopy has provided evidence of silicon on grain facets and at triple points.[12,13] Rao and Schreiker[12] found evidence for a 10 nm wide silicon-rich grain boundary phase based upon a line scan and observed silica at triple points in an yttria PSZ. Drennan and Butler[13] presented similar evidence for silica at triple points and at alumina inclusions in an alumina-doped yttria PSZ.

To summarize, Auger electron spectroscopy was performed on a calcium partially stabilized zirconia. Results of the analysis indicated:

1) a mixture of transgranular and intergranular fracture with extensive porosity on both intergranular and transgranular facets;

2) enhancement of silica and calcium on intergranular facets when compared to transgranular regions;

3) a rapid reduction (over a 1-2 nm distance) of silicon and calcium to bulk values during depth profiling;

4) a possible continuous second phase at grain boundaries; and

5) similar surface chemistry for transgranular and intergranular pores and smooth grain facets.

Acknowledgements

References

1. A. G. Evans and A. H. Heuer, J. Am. Cer. Soc., 63, (1980) 241.

2. R. W. Rice, K. R. McKinney, and R. P. Ingel, J. Am. Cer. Soc., 64, (1981) C-175.

3. L. K. Lenz and A. H. Heuer, J. Am. Cer. Soc., 65, (1982) C-192.

4. L. E. Davis, N. C. MacDonald, P. W. Palmberg, G. E. Riach, and R. E. Weber, Handbook of Auger Electron Spectroscopy (Perkin Elmer, Eden Prairie, Minn., 1978).

5. J. Danielson, J. Vac. Sci. Tech., 20 (1982) 86.

6. G. N. Krishan, B. J. Wood, and D. Cubicotti, J. ElectroChem. Soc., 128 (1981) 191.

7. W. C. Johnson, Met. Trans., 8A (1977) 1413.

8. H. L. Marcus, J. M. Harris, and F. J. Szalkowski, Fracture Mechanics of Ceramics, edited by R. C. Brandt, D.P.H. Hasselman and F. F. Lange, (Plenum Press, NY, 1974), p. 387.

9. J. Drennan, personal communication.

10. J. E. Shackelford, P. S. Nicholson, and W. W. Smeltzer, Am. Ceram. Soc. Bull., 53 (1974) 865.

11. F. F. Lange, J. Am. Cer. Soc., 65 (1982) C24.

12. B. V. Rao and T. P. Schreiber, J. Am. Cer. Soc., 65 (1982) C44 and C195.

13. J. Drennan and E. P. Butler, J. Am. Cer. Soc., 65 (1982) 424 and C194.

APPENDIX

Papers Published/Submitted During 1983

1. J. Lankford, "The Role of Subcritical Tensile Microfracture Processes in Compressive Failure of Ceramics," Fracture Mechanics of Ceramics, Vol. 5, Ed. R. C. Bradt, A. G. Evans, D. P. H. Hasselman, and F. F. Lange, Plenum Press, N.Y., 1983, 625.

2. J. Lankford, "Comparative Study of the Temperature Dependence of Hardness and Compressive Strength in Ceramics," Journal of Materials Science, 18, 1983, 1666.

3. J. Lankford, "Plastic Deformation of Partially Stabilized Zirconia," Journal of the American Ceramic Society, 66, 1983, C-212.

4. J. Lankford, "The Influence of Temperature and Loading Rate on Flow and Fracture of Partially Stabilized Zirconia," Journal of Materials Science (submitted).

5. R. Sherman, "Auger Analysis of Partially Stabilized Zirconia," Journal of Materials Science Letters (submitted).

END

FILMED

3-84

DTIC